DOI: 10.61782/fa.2023.1029

forum acusticum 2023

SOUND-PROPAGATION-MODELS IN WIND-ENERGY: A CODE2CODE-COMPARISON

Katharina Elsen[1*] **Franck Bertagnolio**[2] **Arthur Schady**[1]

[1] German Aerospace Center, Oberpfaffenhofen, Germany
[2] Technical University of Denmark, Roskilde, Denmark

ABSTRACT

Within the framework of IEA wind Task 39 different benchmark-tests are performed. Here we are presenting a comparison of a particle-based model, a wave-based model and a PE-model with respect to two different test cases. They are of theoretical nature, addressing the influence of a simple meteorology in the first case and a simple topography in the second case.

Some non-intuitive behaviour of the models can be observed that is compared for the different models. We will show in particular, how the source (physics or model) of such a behaviour can be analysed and understood. This is important, as some models can create non-physical behaviour – like caustics – whilst at the same time, not all physical effects are captured by different models.

Keywords: *sound propagation simulation, wind energy, code comparison*

1. INTRODUCTION

There are several models currently being used in simulating sound propagation of wind turbine noise, starting from relatively simple standard engineering methods which are also used throughout the planning process of wind parks, up to computationally expensive high fidelity models. Whilst they are all meant to model the same physical process, they can be very different in terms of their physical background, accuracy and computational cost. Most of the models are falling in one of the following categories, which are ray-tracing (or particle tracking), parabolic equations (PE) or Linearized-Euler-Equations (LEE). However, these models do not only differ in terms of their accuracy, they also differ with respect to the sound propagation effects, like refraction or diffraction, that they are able to simulate. Furthermore, one might have to consider peculiarities that come along with the model, like caustic curves in Ray-tracing approaches and a limited propagation angle like in the PE-model. DNS-simulations like the solution to the LEEs on the other hand have the drawback of easily becoming computationally very expensive as the grid width and time resolution have to be adjusted to the wavelength of the highest frequency that is to be modelled. In the following we are presenting three different sound propagation models as well as two theoretical, wind energy related, test cases that were showing interesting and unexpected results. We will then compare the outcome of the simulations and analyse the origin of the effects we are observing.

**Corresponding author*: *katharina.elsen@dlr.de.*

2. DESCRIPTION OF THE 3 MODELS

2.1 Wave-Based Model (*AKU3D*)

The sound propagation model *AKU3D*, described in Blumrich et al [1] and Heimann et al [2], is based on the governing equations of a compressible and adiabatic gaseous medium in a non-rotating system, which are the equation of motion, the equation of continuity and the first law of thermodynamics for adiabatic processes (gravity is

neglected), resulting in the following set of equations:

$$\frac{\partial \mathbf{u}}{\partial t} + (\mathbf{u} \cdot \nabla)\,\mathbf{u} = -\frac{1}{\rho}\nabla p, \tag{1}$$

$$\frac{\partial p}{\partial t} + \mathbf{u} \cdot \nabla p = -\kappa p \nabla \cdot \mathbf{u}, \tag{2}$$

with $\kappa = c_p/c_v$. The atmospheric variables $\phi = (\mathbf{u}, p, \rho)$ are then split up into their meteorological, turbulent and acoustic parts:

$$\phi = \bar{\phi} + \phi' + \phi'', \tag{3}$$

where the overbar ($\bar{\phi}$) denotes the mean variables, a single prime (ϕ') indicates the turbulent deviations from the mean meteorological values and the double prime (ϕ'') describes the deviations from the mean field according to acoustic waves (in particular sound pressure p'' and particle velocity $\mathbf{u}''$).

The sound propagation model is based on prognostic equations of $\mathbf{u}''$ and p''. The model equations are deduced from (1) and (2) with $\mathbf{u} = \bar{\mathbf{u}} + \mathbf{u}''$, $p = \bar{p} + p''$ and $\rho^{-1} = \alpha = \bar{\alpha} + \alpha''$. The equations are then linearized with respect to the mean state where the turbulent parts are disregarded as the atmosphere is seen to be stationary in time. Finally a diffusion term was added in order to simulate the effect of atmospheric absorption.

The prognostic model equations are numerically solved on an orthogonal staggered grid. The numerical scheme conforms to that of the flow model except that the explicit forward-in-time scheme is also used for the diffusion term. The spatial distribution of the meteorological field is taken from the results of a flow model.

2.2 Particle-Based Model (*AKUMET*)

The idea behind the particle-model *AKUMET*, described in Heimann et al [3], is distributing the sound energy on a given number of sound particles and propagating those particles through the atmosphere. The paths of the particles are hereby describing the propagation of the wavefront. *AKUMET* was designed to simulate the propagation of sound over hilly terrain in an inhomogeneous atmosphere. Therefore a frequency-dependent fraction of sound pressure amplitude:

$$p_i(f) = \frac{1}{N}\sqrt{2\rho_s c_s J_0(f)} \tag{4}$$

is assigned to each particle $j (j = 1, \ldots, N)$, where ρ_s and c_s are the air density and sound speed at the source, respectively. The sound intensity at the distance s_0 from the source is given by:

$$J_0(f) = \frac{P_s(f)}{a_1 \triangle \psi s_0^{a1}}. \tag{5}$$

Depending on the type of source, a_1 is set to 2 (point source) or 1 (line source).

The path of the j-th particle is given by the ray vector $\vec{x}_j(t)$ and the unit vector normal to the wavefront $\vec{n}_j(t)$. Differential equations for both vectors are given by Pierce et al [4]:

$$\frac{d\vec{x}_j}{dt} = \vec{v} + c\vec{n}_j, \tag{6}$$

$$\frac{d\vec{n}_j}{dt} = -\vec{\nabla}c - \sum_{i=1}^{3} n_{ji}\vec{\nabla}v_i, \tag{7}$$

with the speed of sound $c = \sqrt{\kappa R_L T}$. $\vec{v}$ is the three dimensional wind vector, whereas κ and R_L are the ratio of specific heat capacities and the gas constant of dry air, respectively. Equations (6) and (7) are numerically integrated for all particles using forward time integration until the particle has left the computational domain.

At the end of the simulation a sound pressure level is computed, based on the particles that have passed through a grid cell during the simulation. The model considers reflection on the ground, air absorption, refraction and obstacles of arbitrary shape. The spatial distribution of the meteorological field is taken from the results of a flow model. The model has already been used in several wind turbine noise applications (e.g. Heimann et at [5]).

2.3 Parabolic Equation (PE) Model

The WindStar-Pro model implements the Generalized Terrain Parabolic Equation (GTPE) as described and tested in Barlas et al [6]. The Helmholtz wave equation is solved for the acoustic pressure in the frequency domain (i.e. independently for each frequency). In the present study, the two-dimensional, wide-angle, Crank-Nicholson, parabolic equation is used with a starter function for modelling a point source. An effective speed of sound, which is the parameter driving sound wave refraction, is used to account for temperature and wind velocity gradients in the atmosphere. The ground impedance is calculated using the classical Delany-Bazley model, which uses the ground flow resistivity as an input. Further implementation details about the PE and GTPE methods are provided in West et al [7] and Salomons [8], respectively.

3. DESCRIPTION OF THE TEST CASES

All together three test cases with different topography and meteorology are studied. These are introduced in the following, in order of their overall complexity.

3.1 Test case 1: Flat topography with generic meteorology

The first test case is characterised by a flat topography and a simple meteorological profile as shown in Fig. 1.

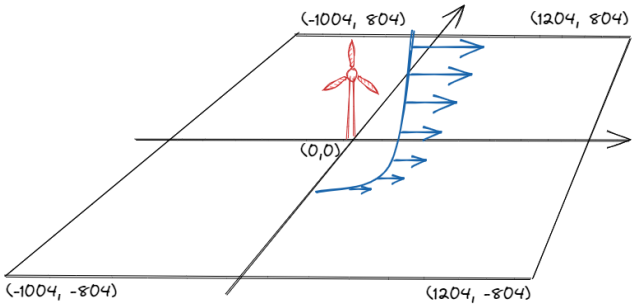

Figure 1. Sketch of computational domain, wind profile and wind turbine position for test case 1.

3.1.1 Topography:

The domain is defined as $[x_{min}, x_{max}] \times [y_{min}, y_{max}] = [-1004\ m, 1204\ m] \times [-804\ m, 804\ m]$ and z ranges from $0\ m$ to $700\ m$. The grid width x/y-direction is given by $d_x = d_y = 8\ m$ and is variable in z-direction (increasing with height).

3.1.2 Meteorology

The parameters of the meteorological profile are given in table 1. The profile is assumed to be constant for all x/y and thus only varies in z. To retrieve the logarithmic wind profile, given a roughness length z_0, the wind speed $u(h)$ for any given height $h > 0$ is calculated from the reference height $h_r > 0$ and reference wind speed u_r as follows:

$$u(h) = u_r \frac{\ln\left(\frac{h}{z_0}\right)}{\ln\left(\frac{h_r}{z_0}\right)} \tag{8}$$

3.1.3 Source:

The wind turbine is located at $(x_0, y_0) = (0, 0)$ and is defined as a single point source at $78\ m$ over ground, with a sound power level of $107\ dB$. Simulations with a spectrum of frequencies from $20\ Hz$ to $20\ kHz$ as well as single frequency simulations were performed. For this paper, frequencies of 16 Hz and 100 Hz are used.

3.1.4 Model setup:

The simulation was performed without turbulence, using standard air absorption (ISO 9613) and totally even ground. The ground itself was considered using complex impedance and diffraction at the ground was enabled.

3.2 Test case 2: Single hill with meteorology

The second test case is a 2D-domain characterised by a hill and a simple meteorological profile as shown in Fig. 2.

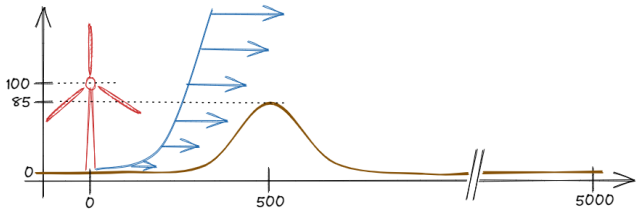

Figure 2. Sketch of topography, wind profile and wind turbine position for test case 2.

3.2.1 Topography:

The domain is defined by $[x_{min}, x_{max}] = [0\ m, 5000\ m]$ and z ranges from $0\ m$ to $1500\ m$. The height of the hill itself is defined in (9).

$$h(x) = 84.9 \cdot \exp\left(-\left(\frac{x - 500}{200}\right)^2\right). \tag{9}$$

The grid width depends on the model. In case of the particle-model $d_x = 8\ m$ was sufficient, whereas it is variable in z-direction (increasing with height). For the wave-based-model $d_x = d_z = 1.5$ was chosen.

3.2.2 Meteorology

The parameters of the meteorological profile are given in table 1 on the right. The profile is assumed to be constant for all x and thus only varies in z. The wind profile with

Table 1. Meteorology for test cases 1 (left) and 2 (right).

Case 1			Case 2		
parameter		value			
sound speed	$[m/s]$	340.0	sound speed	$[m/s]$	340.0
temperature	$[°C]$	20.0	temperature	$[°C]$	15.0
vertical temp. grad.	$[K/100m]$	0.0	vertical temp. grad.	$[K/100m]$	0.0
humidity	$[\%]$	70.0	humidity	$[\%]$	70.0
wind speed in 10 m	$[m/s]$	(0.0/2.5/)5.0	wind speed in 100 m	$[m/s]$	8.0
wind profile		log. prof.	wind profile		power law
roughness length	$[m]$	0.2	power coefficient		0.143
wind direction	$[°]$	270.0	wind direction	$[°]$	270.0
ground resistivity	$[kPas/m^2]$	absorption	ground resistivity	$[kPas/m^2]$	250.0

wind speed $u(h)$ at a given height h was calculated using the power law:

$$u(h) = u_r \left(\frac{h}{h_r} \right)^{\beta} \tag{10}$$

with power coefficient β, reference height $h_r > 0$ and reference wind speed u_r.

3.2.3 Source:

The source is located at $x_0 = 0$ and is defined as a single point source. Three simulations where performed with the respective height of the source at $z = 30, 100, 300\ m$. Several frequencies have been tested, here we will concentrate on 16 Hz.

3.2.4 Model Setup:

4. SIMULATION RESULTS

In the following three subsections we are showing the simulation results of the test cases described above, i.e. describing the initial problem, explaining the thought-process to narrow down the problem and finally comparing the results obtained using the different models.

4.1 Flat topography with generic meteorology

4.1.1 Description of the problem

The Problem was initially found during *AKUMET*-Simulations for wind-turbine noise. A 2D-plot of the associated sound pressure level on the ground is shown in Fig. 3. The wind direction is 270°, i.e. the wind is blowing in positive x-direction. As can be expected, the

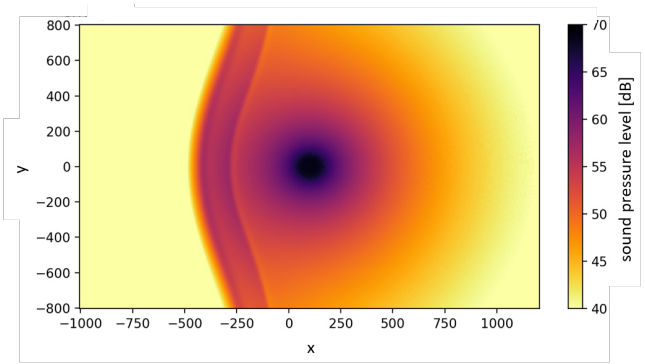

Figure 3. 2D-plot of the sound pressure level simulated on the ground using *AKUMET* for the first test case.

sound pressure level in the downwind-domain is generally higher than in the upwind-domain. The shadow-zone in the upwind-domain is clearly visible. However, there is also a strong increase in sound pressure level visible directly before the beginning of the shadow zone whose origin is not obvious.

4.1.2 Solution strategies

To narrow down the problem, we first reduced it to the 2D-domain and disabled several subroutines connected to weighting and smoothing the sound pressure level. Further we switched to fully absorbing ground conditions to eliminate reflections. As the problem is obviously dependent on the wind field, we then performed simulations

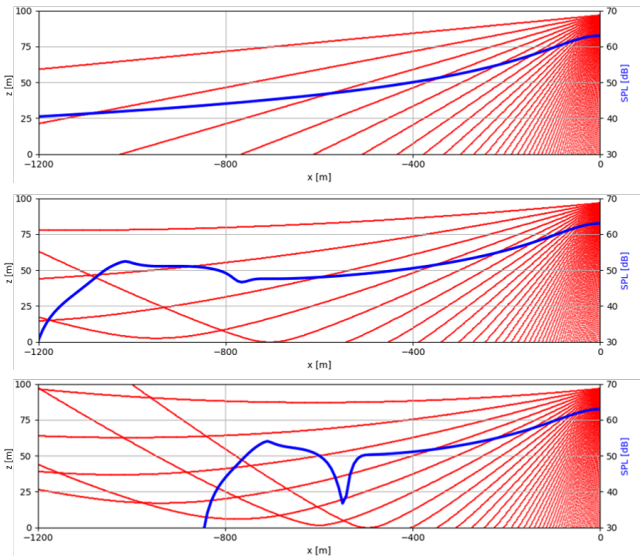

Figure 4. Results for test case 1, computed using *AKUMET* for three different wind speeds (top: 0 m/s, middle: 2.5 m/s, bottom: 5/s) with a grid width of 8 m for a frequency of 100 Hz. Sound pressure level is given in blue, sound rays are shown in red.

with different wind speeds. The main goal was to understand whether the origin of the effect was physical, numerical or model-related. As *AKUMET* is basically a Ray-tracing-model, we were able to plot those rays, which are essentially the paths that the particles are travelling. The results, restricted to the upwind-domain, for different wind speeds are shown in Fig. 4. The sound pressure level is shown in blue whereas selected sound rays are plotted in red. No wind speed is given in the top figure, lower wind speed (2.5 m/s) was chosen in the middle figure and the original wind speed (comp. table 1) was used for the bottom figure.

4.1.3 Explanation of the effect

From Fig. 4 can be seen that the increase of sound pressure level is preceded by a sudden drop of it. The effect, including the depth of the drop, clearly increases with the wind speed and it occurs earlier on in the domain the higher the wind speed is while it is absent in the absence of wind. This is easily explained by the stronger downwards refraction of the sound rays in higher wind speeds. It shall however been mentioned that the effect is not exactly related to the wind speed itself but to the wind speed

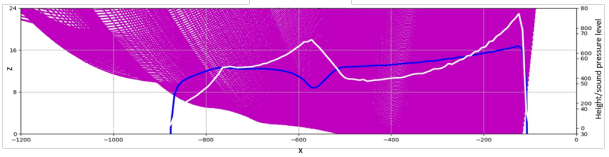

Figure 5. Results for test case 1, computed using *AKUMET* with a grid width of 8 m for a frequency of 100 Hz. Sound pressure level is given in blue, sound rays are shown in purple and the number of particles per grid cell in white.

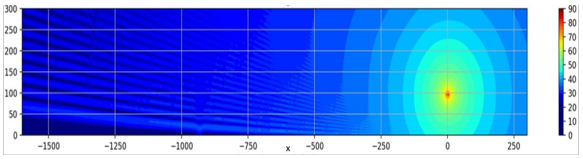

Figure 6. Sound pressure level field for test case 1, computed using *AKU3D* for a frequency of 100 Hz and a wind speed of 5 m/s.

gradient.

Looking more closely at the sound rays we find that the drop occurs in the area where the first sound rays, those still moving downwards and those already been refracted upwards, are intersecting. This leads, on one hand, to a higher number of particles in that area, and on the other hand, to destructive interference (resulting in the sound pressure level to drop, blue curve). This can be seen in Fig. 5 (sound rays are shown in purple to indicate the beginning of the shadow zone), where the number of particles is indicated by the white curve, the sound pressure level is again shown in blue. Further downwind the number of particles decreases again but so do the effects of interference, leading to an increase in sound pressure level. The number of particles is, due to the additional, upwards refracted sound rays in that area, still higher than it was before the drop, and therefore is the sound pressure level. Finally, the maximum in sound pressure level (around x=-700 in Fig. 4, bottom) is caused by constructive interference. These results are obtained under the assumption of a coherent source.

4.1.4 Comparison with other model results

The input parameters of *AKUMET* cannot be matched exactly on the wave-based model *AKU3D*, as, one being a

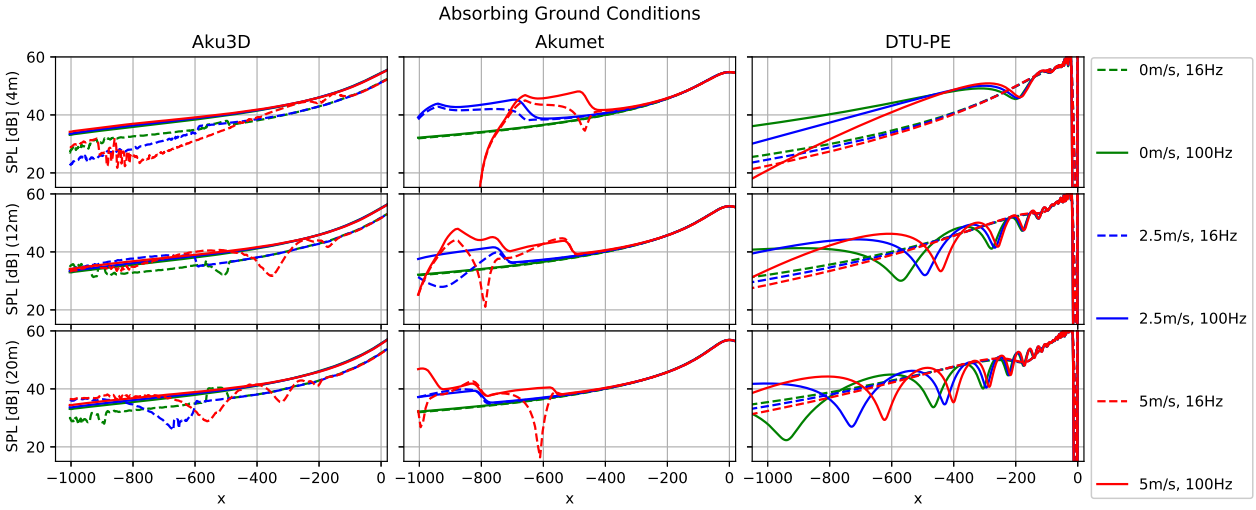

Figure 7. Test Case 1, absorbing ground conditions: left: Aku3d, middle: Akumet, right: PE; from top to bottom: 4m, 12m and 20m above ground; dashed and solid line: 16 Hz and 100Hz respectively; green, blue and red: 0m/s, 2.5m/s and 5m/s wind speed

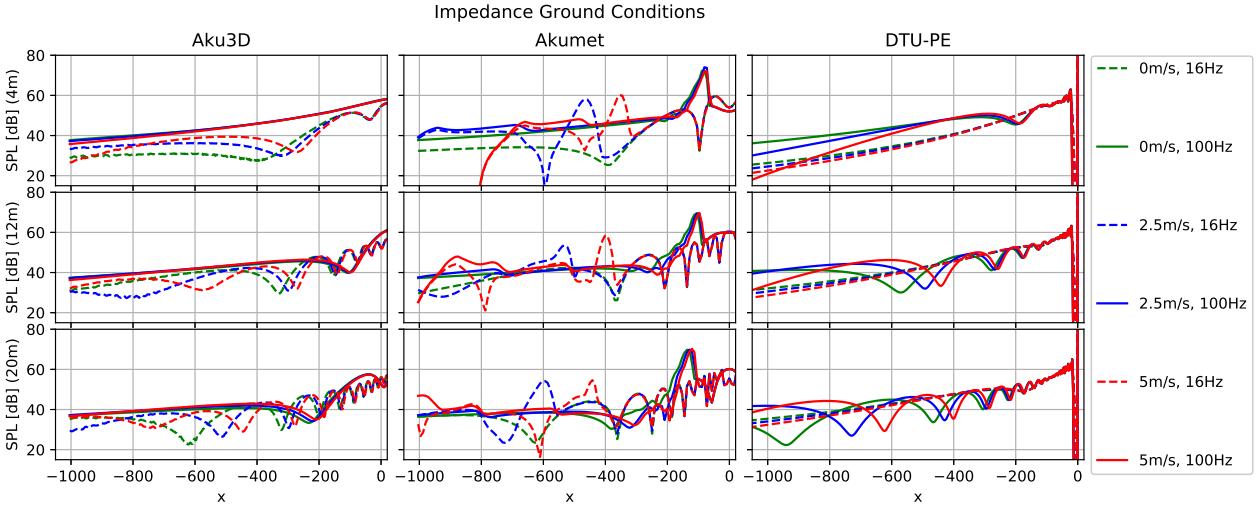

Figure 8. Test Case 1, impedance ground conditions: left: Aku3d, middle: Akumet, right: PE; from top to bottom: 4m, 12m and 20m above ground; dashed and solid line: 16 Hz and 100Hz respectively; green, blue and red: 0m/s, 2.5m/s and 5m/s wind speed

Lagrangian approach and the other a Eulerian approach that directly simulates the wave propagation, they have different requirements concerning e.g. grid width and time stepping. The same holds for the PE-model. Therefore the input parameters were adapted to fit the model. Due to the high computational cost the domain was restricted to 2D. The resulting sound pressure level field of the *AKU3D*-simulation is shown in Fig. 6. One can nicely see the interference pattern, as well as the formation of a shadow zone in the upwind domain. Fig. 7 shows the behaviour for 3 different wind speeds (0 m/s, 2.5 m/s and 5 m/s) and two different frequencies (16 Hz and 100 Hz) for all three models using absorbing boundary conditions. Fig. 8 shows the same test case for impedance boundary conditions. Clear differences can be observed between the models, for different frequencies, but also between impedance and absorbing ground conditions. Generally, the results of *AKU3D* and *PE-DTU* are more similar to each other, while in case of *AKUMET* the wave can be observed more clearly. Simulations with absorbing ground are strongly helping in understanding the origin of the problem, as in case of impedance boundary conditions – due to the single frequency – reflection patterns can be observed. Nonetheless, the wave can be observed with all three models. The reason why the wave is more pronounced in case of the *AKUMET*-simulation is most likely explained by the formation of a shadow zone, leading to sharper edges (comp. Fig. 4).

4.2 Single hill with simple meteorology

In Fig. 9 the original findings of test Case 2 for 16Hz and a source in 30m of height are shown for different models (PE, Nord2000) as well as for different turbulence settings, geometric spreading is shown in grey (solid). No legend is given in this plot as we only want to point out the initial problem, which is the second drop in sound pressure level, followed by a rise in the sound pressure level. Whilst the first drop is easily explained by the shadow zone, formed by the hill (shown in light grey), the explanation of the second drop is less obvious. There are also significant differences between the different models. Fig. 10 shows a comparison of the simulations results for the three models compared in this paper. From left to right we find the results of *AKU3D* *AKUMET* and *PE-DTU* each for three different source heights, 30m (dashed, green), 100m (solid, blue) and 300m (dotted, red) and all for a frequency of 16 Hz. It shall be noted that the results are still preliminary and only a qualitative comparison can be made between the models. The three models are showing significant differences but also some similarities. The largest differences are found for the 30m source, as here the influence of the hill is strongest, due to the formation of a shadow zone. Due to computational limitations, only the domain up to 1350m is shown here, however, this includes the area of the second drop of the *PE-DTU*-model. Such a drop could not be found in case of *AKU3D* for neither of the source heights. In case of *AKUMET* we find some oscillations in the far field of the 100m source that result from numerical limitations. Only the *AKUMET*-simulation is showing the building of a sharp shadow-zone in case of the 30m source. Comparing the results to test case 1, one could assume that the drops in the *PE-DTU*-simulation result from interference-effects. Also in test case 1, interference and reflection effects where varying significantly in all three simulations. However, we can not yet prove this assumption and further analysis has to be done to fully explain the effect.

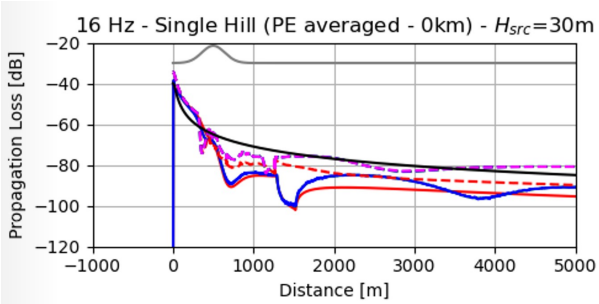

Figure 9. Test Case 2, 16Hz, original findings: comparison of the results of the 30m source height for different models (PE, Nord2000) and different turbulence settings, geometric spreading is shown in grey (solid)

5. SUMMARY

We were presenting two theoretical test cases and comparing the according simulation results of three different sound propagation models. In particular in test case 1, the questionable behaviour could be observed – from a qualitative point of view – in all three models, also significant differences were found among the respective simulations. It was shown how the origin of a specific behaviour can be traced down using the specific characteristics (i.e. sound rays) of the different sound propagation

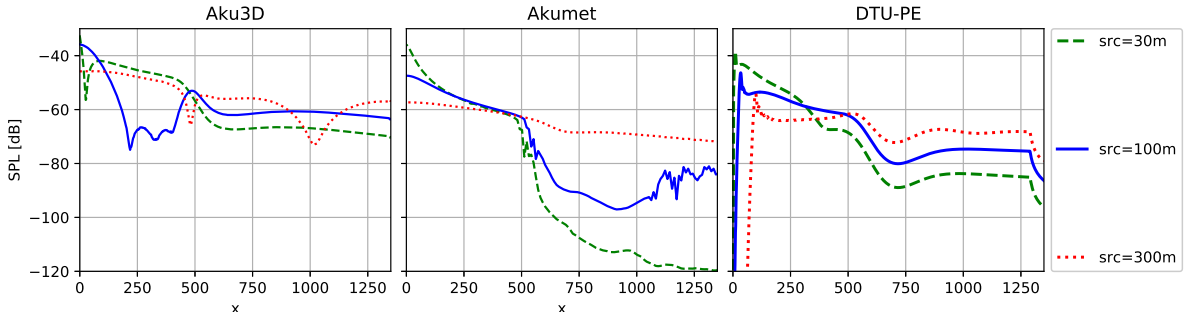

Figure 10. Test Case 2, impedance ground conditions, 16Hz: left: Aku3d, middle: Akumet, right: PE; dashed (green), solid (blue) and dotted (red) line: source height of 30m, 100m, and 300m respectively

models. With respect to the second test case more detailed analysis of the problem has to be done to fully understand the origin of the problem. Generally speaking, all models do have their advantages and disadvantages and our findings are showing that it can be beneficial to use different model-approaches to simulate a specific problem. This can strongly help the investigation whether a problem is really physical or model related.

6. REFERENCES

[1] R. Blumrich and D. Heimann, "A linearized eulerian sound propagation model for studies of complex meteorological effects," *JASA*, vol. 112, no. 2, pp. 446–455, 2002.

[2] D. Heimann and R. Karle, "A linearized euler finite-difference time-domain sound propagation model with terrain-following coordinates," *JASA*, vol. 119, no. 6, pp. 3813—-3821, 2006.

[3] D. Heimann and G. Gross, "Coupled simulation of meteorological parameters and sound level in a narrow valley," *applied acoustics*, vol. 56, pp. 73–100, 1999.

[4] A. D. Pierce and P. W. Smith, "Acoustics: An introduction to its physical principles and applications.," *Physics Today*, vol. 34, no. 12, pp. 56–57, 1981.

[5] D. Heimann, Y. Käsler, and G. Gross, "The wake of a wind turbine and its influence on sound propagation," *MetZet*, vol. 20, no. 4, pp. 449–460, 2011.

[6] E. Barlas, W. J. Zhu, W. Z. Shen, K. O. Dag, and P. Moriarty, "Consistent modelling of wind turbine noise propagation from source to receiver," *J. Acoust. Soc. Am.*, vol. 142, no. 5, pp. 3297–3310, 2017.

[7] M. West, K. Gilbert, and R. A. Sack, "A tutorial on the parabolic equation (pe) model used for long range sound propagation in the atmosphere," *Appl. Acoust.*, vol. 37, no. 1, pp. 31–49, 2017.

[8] E. M. Salomons, *Computational Atmospheric Acoustics*. Netherlands: Springer Dordrecht (Publisher), 2002.